Tuning the interfacial stoichiometry of InP core and InP/ZnSe core/shell quantum dots

Nayon Park, Forrest W. Eagle, Asher J. DeLarme, et al.

COLLECTIONS

Paper published as part of the special topic on From Atom-Precise Nanoclusters to Superatom Materials

View Online   Export Citation   CrossMark

ARTICLES YOU MAY BE INTERESTED IN

Effects of Zn^{2+} and Ga^{3+} doping on the quantum yield of cluster-derived InP quantum dots
The Journal of Chemical Physics **151**, 194702 (2019); https://doi.org/10.1063/1.5126971

Effect of indium alloying on the charge carrier dynamics of thick-shell InP/ZnSe quantum dots
The Journal of Chemical Physics **152**, 161104 (2020); https://doi.org/10.1063/1.5145189

The effect of nanocrystal surface structure on the luminescence properties: Photoemission study of HF-etched InP nanocrystals
The Journal of Chemical Physics **123**, 084706 (2005); https://doi.org/10.1063/1.2004901

AIP Publishing

Tuning the interfacial stoichiometry of InP core and InP/ZnSe core/shell quantum dots

Nayon Park, Forrest W. Eagle, Asher J. DeLarme, Madison Monahan, Talia LoCurto, Ryan Beck, [iD]
Xiaosong Li, [iD] and Brandi M. Cossairt[a) [iD]

AFFILIATIONS

Department of Chemistry, University of Washington, Seattle, Washington, 98195-1700, USA

Note: This paper is part of the JCP Special Topic on From Atom-Precise Nanoclusters to Superatom Materials.
[a)]Author to whom correspondence should be addressed: cossairt@uw.edu

ABSTRACT

We demonstrate fine-tuning of the atomic composition of InP/ZnSe quantum dots (QDs) at the core/shell interface. Specifically, we control the stoichiometry of both anions (P, As, S, and Se) and cations (In and Zn) at the InP/ZnSe core/shell interface and correlate these changes with the resultant steady-state and time-resolved optical properties of the nanocrystals. The use of reactive trimethylsilyl reagents results in surface-limited reactions that shift the nanocrystal stoichiometry to anion-rich and improve epitaxial growth of the shell layer. In general, anion deposition on the InP QD surface results in a redshift in the absorption, quenching of the excitonic photoluminescence, and a relative increase in the intensity of broad trap-based photoluminescence, consistent with delocalization of the exciton wavefunction and relaxation of exciton confinement. Time-resolved photoluminescence data for the resulting InP/ZnSe QDs show an overall small change in the decay dynamics on the ns timescale, suggesting that the relatively low photoluminescence quantum yields may be attributed to the creation of new thermally activated charge trap states and likely a dark population that is inseparable from the emissive QDs. Cluster-model density functional theory calculations show that the presence of core/shell interface anions gives rise to electronic defects contributing to the redshift in the absorption. These results highlight a general strategy to atomistically tune the interfacial stoichiometry of InP QDs using surface-limited reaction chemistry allowing for precise correlations with the electronic structure and photophysical properties.

Published under an exclusive license by AIP Publishing. https://doi.org/10.1063/5.0060462

INTRODUCTION

Advances in the synthetic optimization of InP-based quantum dots (QDs) have led this material to a position of prominence for commercial display applications.[1–6] Recent demonstrations of near-unity quantum yield and >20% external quantum efficiency in electroluminescent devices have placed InP on par with cadmium-based quantum dot emitters.[7,8] The chemical design principles that underlie these advances, however, remain poorly understood. The atomistic synthesis of colloidal quantum dots that are defect-free, both structurally and electronically, has long been a topic of fundamental research and remains so even today. Typical solution-based hot injection and heat-up synthesis methods generate quantum dots that are marred by surface defects that create electronic trap states within the semiconductor bandgap.[9–14] These mid-gap states introduce both radiative and non-radiative relaxation pathways that compete effectively with the desired band-edge recombination process. Consequently, the need to understand and modulate the surface chemistry that governs these photophysical properties has risen to paramount importance in the field.

The effects of surface passivation and ligand type on photoluminescence (PL) and charge transfer properties have been abundantly reported.[15–23] Recent studies on InP-based core/shell quantum dots have reported a diverse set of factors affecting the photoluminescence properties of emissive InP QDs, including uniformity of the InP core,[24,25] thickness and composition of the zinc chalcogenide shell,[24–26] electron and hole wavefunction overlap,[24,25] surface defects (such as oxidized species or dangling bonds),[7,23] and stacking faults at the core/shell interface due to lattice mismatch.[27,28] The achievement of 100% photoluminescence quantum yield (PL QY) has been attributed to well-confined electron and hole

wavefunctions through engineering the inner shell layer,[25,29] the removal of oxidative defects by etching with HF prior to shelling,[7] a well-passivated surface on a stoichiometric InP core,[8] and the removal of indium defects in the shell by an additional washing step.[8,30] The high sensitivity of optical properties to the core stoichiometry and interface morphology has been highlighted in recent computational studies.[31,32] These considerations are influenced by the composition and the chemical environment at the core/shell interface, highlighting the need for further investigation on the nature of surface trap states and how to deterministically treat the quantum dot core en route to highly emissive, defect-free core/shell QDs.

In this study, we have sought to modify the interfacial stoichiometry of emissive InP QDs using surface-limited reaction chemistry to correlate interfacial composition with the PL properties of the resulting core and core/shell materials. Reactive silyl reagents containing the desired anion (P, Se, S, or As) were added to In-rich InP QDs capped with carboxylate ligands to obtain substoichiometric to anion-rich cores. Optical spectroscopy of the resultant core QDs indicates delocalization of the exciton wavefunction and relaxation of exciton confinement. The efficacy of the reactive silyl reagents in shifting the stoichiometry of shelled QDs and their impact on improving the epitaxial growth to reduce ensemble heterogeneity were demonstrated. Time-resolved photoluminescence (TR PL) spectroscopy revealed that interfacial modulation of InP/ZnSe QDs results in similar decay dynamics on the ns timescale, suggesting that changes in PL QY can be attributed to new defect-related pathways related to hole trapping on the ps timescale promoting non-radiative recombination. Further insight into the effects of surface stoichiometry of InP/ZnSe core/shell QDs was gained from analogous shelling experiments starting with purified Zn-treated InP QDs, which exhibited no notable differences from starting with In-rich InP QDs in the final PL traces, suggesting that the role of Zn in the QD core in the final heterostructures is relatively insignificant compared to the immediate interface the core surface forms with the shell layer. The dynamics in all of these systems were found to be remarkably similar, and low temperature PL data support the prevalence of a trap-mediated non-radiative recombination process. The decreased PL QYs also suggest the presence of a population of dark non-emissive QDs in the ensemble bearing a shifted interface stoichiometry. Density functional theory (DFT) results indicate that modification of the stoichiometric composition at the core/shell interface can lead to the appearance of shallow hole traps dependent on the identity of the anion. These results highlight the role of the atomic composition of the QD core/shell interface and motivate further exploration of complex material systems fabricated through atomistic reaction chemistry.

RESULTS AND DISCUSSION

Anion-rich InP core QDs

First, In-rich, carboxylate-capped InP core QDs were synthesized from atomically precise $In_{37}P_{20}(O_2R)_{51}$ ($R = C_{18}H_{33}$; oleate) clusters and purified to make a stock solution with a known In concentration. These InP cores were dried and redissolved in trioctylamine. Trioctylamine has recently gained traction in the synthesis of highly emissive InP-based quantum dots

for its high boiling point (365–367 °C) and ease of removal with alcohol-based anti-solvents.[4,7] In this reaction, it serves a double duty of maintaining the colloidal stability of the quantum dots upon surface treatment while circumventing surface etching that is observed with primary amines (Fig. S1).

Reactive trimethylsilyl (SiMe$_3$, TMS) reagents containing the desired pnictide (P and As) or chalcogenide (S and Se) anion was suspended in trioctylamine. Half an equivalent of anion relative to In was used to yield InP cores with a maximally modified surface stoichiometry as determined by inductively coupled plasma-optical emission spectroscopy (ICP-OES, Table I). The addition of P(SiMe$_3$)$_3$ yielded particles that were still In-rich but had a shifted stoichiometry of 1:0.8 In to P ratio, a 33% increase from the starting 1:0.6 ratio of InP QDs. An upper limit of 1:1.4 for the In:P ratio for a P-rich InP core that originally has a 3.1 nm diameter was extrapolated from QD modeling by Zhao and Kulik[33] by adding an equivalent anion excess relative to the number of excess In ions (calculations shown in the supplementary material, Text S1). For TMS arsenide, sulfide, and selenide, the surface reaction resulted in nanocrystals that exhibited a decrease in P content relative to In, while the added anions were present at a ratio that is almost equivalent to In and an overall cation to anion ratio of 1:1.3–1:1.4.

Using ^{1}H nuclear magnetic resonance (NMR) spectroscopy, the reaction at the InP surface was further probed [Fig. 1(a)]. As-synthesized InP QDs can most simply be described as a stoichiometric core and an In-rich surface, capped by long chain carboxylate as the native ligand that is available for surface-limited reaction with the TMS reagent (Scheme 1). In this setup, the reaction is expected to stop when all of the surface carboxylates (i.e., possible reaction sites) are consumed, eliminating further formation of TMS ester that drives the reaction forward. A stock of InP QDs was further purified by gel-permeation chromatography (x2) to ensure the removal of any excess ligands. The presence of a broad peak (δ = 5.6–6.0 ppm) indicating bound oleate was confirmed. This peak shifts to ~5.3–5.6 ppm in the presence of trioctylamine. The reaction of purified InP QDs with P(SiMe$_3$)$_3$ shows growth of TMS ester over the course of the reaction with a concurrent decrease in the phosphine precursor peak, demonstrating that the reaction is occurring between the surface bound In carboxylate and P(SiMe$_3$)$_3$. Additionally, HP(SiMe$_3$)$_2$ is a known protonolysis product of P(SiMe$_3$)$_3$ and has been previously reported to be involved in competing precursor conversion pathways in the growth of InP quantum dots.[34] Even when all excess acids are removed from the InP QDs during purification, carboxylic acids are able to remain bound to the

TABLE I. ICP-OES results showing In:P:E (E = As, S, and Se) ratio of as-synthesized and surface anion-treated InP QDs normalized to In.

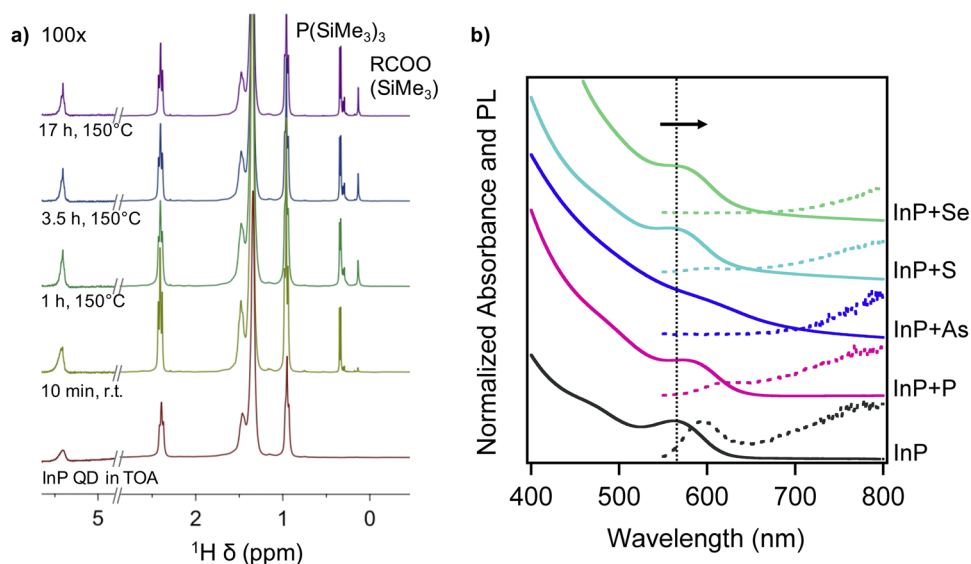|	In	P	As	S	Se	In:anion
InP	1	0.6				1:0.6
InP + P	1	0.8				1:0.8
InP + As	1	0.5	0.9			1:1.4
InP + S	1	0.4		0.9		1:1.3
InP + Se	1	0.4			0.9	1:1.3

FIG. 1. InP QD surface treatment with TMS anion reagents. (a) ^{1}H NMR spectra showing the evolution of the reaction of carboxylate-capped InP QD with P(SiMe$_3$)$_3$ obtained (300 MHz, C$_6$D$_6$, 298 K, delay time of 20 s). The oleate peak centered around 5.5 ppm was amplified by 100× for visibility. (b) UV–vis (solid) and PL (dotted) spectra of native (black), P (pink), As (navy), S (teal), and Se-treated (green) InP QDs. The vertical dotted line indicates the absorbance max of the native InP QD to guide the eye for redshifted absorbance of anion-treated InP QDs.

surface through L-type coordination as has been evidenced by detailed NMR studies.[35,36] While the reaction hardly proceeds at room temperature, after one hour at 150 °C, the reaction is mostly complete. The reaction of surface carboxylates and TMS phosphine proceeds and halts before all of the phosphine precursor is consumed, confirming that the reaction of P(SiMe$_3$)$_3$ remains limited to the QD surface. The reaction yield of TMS ester is ~40%, while 45% of the P(SiMe$_3$)$_3$ remains unreacted, which is in agreement with the ICP-OES results. Additional evidence for the removal of the native carboxylate ligands is the evolution of a multimodal resonance that includes a sharp component in the alkene region as the ligand becomes unbound from the nanocrystal surface and forms TMS ester. Similarly, the reaction of purified InP QDs with Se(SiMe$_3$)$_2$ was monitored by ^{1}H NMR spectroscopy. The conversion yield of TMS selenide was calculated to be 65%, which is significantly higher

than that of P(SiMe$_3$)$_3$ and is consistent with the high ratio of Se incorporated in the surface-modified InP QDs from the ICP-OES results (Table I).

The observed optical properties from UV–Vis and PL spectroscopy reveal a redshift by 17 nm with the addition of P(SiMe$_3$)$_3$ [Fig. 1(b)], which can be attributed to the growth of the InP core as previously reported in the literature.[8] The excitonic PL intensity was diminished without significantly perturbing the broad, redshifted trap PL. This characteristic trap PL feature of InP QDs has previously been ascribed to the emission from hole trap states arising from surface P dangling bonds.[14] The addition of As(SiMe$_3$)$_3$ to the InP core resulted in a similar redshifted absorbance and quenching of excitonic PL while trap PL persisted, although the absorbance peak appeared qualitatively much less defined. This broadened absorbance can be attributed to
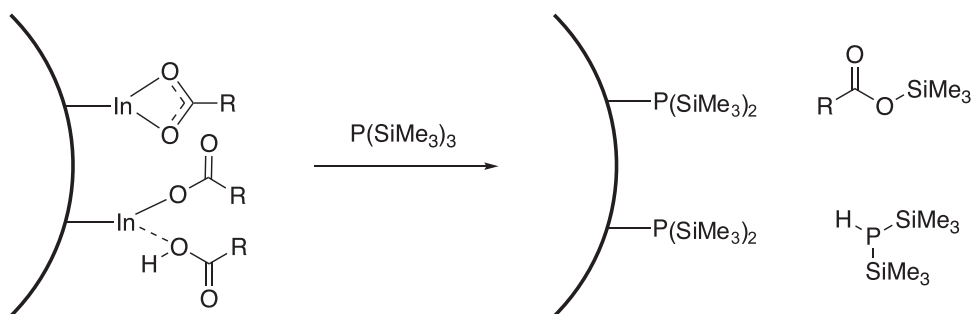
SCHEME 1. Proposed surface reactions between carboxylate/carboxylic acid-capped InP QDs and P(SiMe$_3$)$_3$.

alloying of the phosphorus and arsenic anions and reflects the ease of arsenic incorporation in the InP core QD, as has been previously reported.[37]

The addition of bis(trimethylsilyl) sulfide (or selenide) afforded S- (or Se-) treated anion-rich InP cores. The formation of InP cores with these chalcogenides coating the surface is of interest as they are commonly used as a component of the wide bandgap shell material, including Zn and Cd chalcogenides. Both S- and Se-treated InP cores exhibited a redshift in the absorbance, while the excitonic PL was significantly diminished [Fig. 1(b)]. The broad, redshifted trap PL persisted for both, remaining as a notable feature of these core QDs with anion-rich surfaces.

Structural characterization of the surface-modified InP cores by powder X-ray diffraction (XRD, Fig. S2) confirms that these core QDs retain the zinc blende InP structure with no observable change in FWHM. It is worth noting that the (111) plane of the S-treated core shifts to higher 2θ by 0.4°, suggestive of a contracted lattice due to the surface strain by the smaller S atoms. TEM (transmission electron microscopy) images corroborate no notable changes in the size of the nanocrystals from the original 3.1 nm diameter (Fig. S3).

With the knowledge that the surface anion treatment did not change the size, morphology, or the crystal structure of the InP QDs to any significant degree, the observation of the redshift in the absorbance can be attributed to a change in the electronic structure as a result of the shifted stoichiometry. More specifically, the redshift suggests a quasi-Type II band structure, where delocalization of the charge carrier wavefunction results in relatively softer confinement of the exciton in the core. This is consistent with theoretical investigations by Rodosthenous et al.,[31] who concluded that P-rich InP QDs have delocalized electrons and localized holes, resulting in an overall decreased wavefunction overlap. Similar phenomena have been reported by Buckley et al. where the observed redshifts with chalcogenol ligands installed on the surface of CdSe QDs were attributed to relaxed quantum confinement resulting from the coupling between the highest occupied molecular orbital (HOMO) of the chalcogenol and the QD hole wavefunction.[38] It was proposed that chalcogenol ligands attract the hole and localize hole density at the surface. Where this observation becomes more nuanced is that such separation of the electron and hole simultaneously results in a reduction in the Coulombic interaction. The decreased exciton binding energy is expected to cause a blueshift. Recently, the effect of accounting for this Coulombic interaction between the electron and the hole to calculate the bandgaps of II–VI QD heterostructures was demonstrated using Poisson's equation in an effective mass approximation.[39] With this, we note that III–V semiconductor materials typically exhibit small effective masses,

which means that the Coulombic energy accounts for only a small fraction of the bandgap energy.[40] Because spatial separation of the exciton would result in a reduction in exciton wavefunction overlap, the quenching of excitonic PL is expected, and we propose this as a reasonable explanation for the PL quenching we observe in the anion-treated InP cores.

Anion-rich interface in core/shell QDs

In situ shelling of the anion-rich InP QDs was performed to investigate the effects of the modified interfaces on the luminescence and photophysical properties of the core/shell QDs. A wider bandgap ZnSe shell for type-I band alignment (confinement of exciton to the core) with InP was chosen to standardize the shelling procedure, for structural simplicity, and a better lattice match with the InP core compared to ZnS (lattice mismatch of 3.4% vs 7.7%). Shelling was carried out (Scheme 2) by first taking purified InP QDs dissolved in trioctylamine and slowly injecting 0.5 equivalent (vs In) of the reactive silyl reagent containing P, As, Se, or S at 150 °C for an hour. A ZnSe shell was grown on the surface-modified cores using temporally separated slow injection of Zn and Se precursors, each at 220 and 300 °C, respectively. The excitonic PL was recovered for all samples upon the addition of Zn and continued to increase in intensity throughout the growth of the ZnSe shell. The observation of increased PL intensity upon the addition of Zn can be attributed to the passivation of the surface anion sites that serve as hole traps as has been seen previously in both II–VI and III–V systems.[13,41]

The resultant InP/ZnSe core/shell QDs exhibited varying PL efficiencies and a range of absorption and PL wavelengths. The highest PL QY of 41% straight out of synthesis was achieved by the control sample where no interfacial anion was added prior to shelling. The PL QY was improved to 75% upon initial purification, likely due to the removal of a population of unshelled InP QDs. Initial purification involved centrifuging the concentrated sample from vacuum distillation diluted with toluene to remove the insoluble fraction. The supernatant was then flushed with acetonitrile and was centrifuged once more to remove any remaining reaction by-products. This procedure effectively separates the aggregated, oxidized, and otherwise scattering materials, which has the net effect of improving the ensemble quality and the quantum yield. This PL QY was reduced to 15% upon size-selective precipitation that narrowed the emission linewidth. While repeated centrifugation–precipitation–redissolution cycles can strip off the surface ligands and lower the PL QY, size-selective precipitation was necessary to proceed with further characterization of these
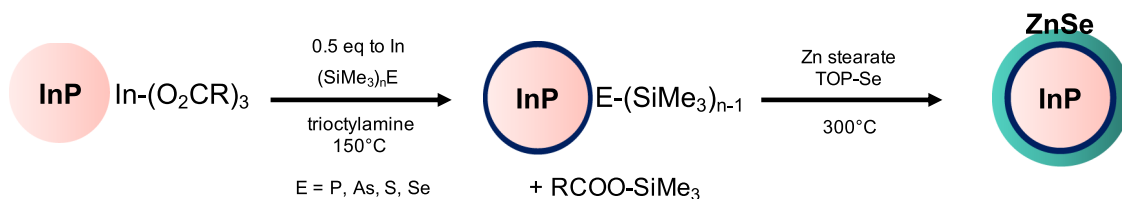
SCHEME 2. Shelling scheme of interface controlled InP/ZnSe QDs.

samples to probe the impact of interfacial stoichiometry in a homogeneous population. The change in emission linewidth following size-selective precipitation was most pronounced in the control sample, suggesting heterogeneous shell growth that results in the broadening of the linewidth. The normalized PL spectra of all samples before and after size-selective precipitation are shown in Fig. 2(a). Notably, the PL linewidth and the line shape showed minimal change after size-selective precipitation for the As, S, and Se-rich interface core/shell QDs, suggesting a more controlled and uniform growth upon synthesis compared to the traditional shelling approach.

Further insight was gained from elemental and structural analysis of the shelled particles purified by size-selective precipitation. Elemental analysis by ICP-OES indicated retention of the anions that were post-synthetically added to the purified InP QD surface (Table II). The P-treated interface resulted in an In:P ratio of 1:1. It is evident from the atomic ratios that the anions employed in core surface treatment were incorporated in the final core/shell

TABLE II. The atomic compositions of InP/ZnSe QDs with anion-modulated interfaces obtained from ICP-OES. The molar ratios are normalized to moles of In.

	In	P	As	S	Se	Zn
InP/ZnSe	1.0	0.3			6.8	7.1
InP + P/ZnSe	1.0	1.0			5.2	5.8
InP + As/ZnSe	1.0	0.3	2.7		5.6	5.0
InP + S/ZnSe	1.0	0.5		1.0	3.8	4.6
InP + Se/ZnSe	1.0	0.4			9.1	8.6

structure, with the ratio of the shelling layer representative of a 1–2 monolayer shell. The expected core/shell structure is corroborated by powder XRD [Fig. 3(a)], where the zinc blende InP/ZnSe QD structure is observed across all samples, with the InP reflections exhibiting shifts toward bulk ZnSe, indicating successful shelling and reliably homogeneous populations following size-selective precipitation. For the sample with a P-rich interface, the asymmetry of the peaks at 43.6° (220) and 51.7° (311) may be attributed to stacking disorder within the nanocrystal.[42,43] We propose that inhomogeneous strain due to uneven compositional distribution or alloying can give rise to defect-related nonradiative recombination. TEM analysis shows nanocrystals of sizes between 7.0 and 7.5 nm in diameter and highly crystalline lattices despite their irregular morphology [Figs. 3(b)–3(f)].

These samples were further probed by time-resolved photoluminescence spectroscopy (TR PL) to study the effects of the modified interfaces on the charge carrier dynamics [Fig. 2(b) and Table III]. The PL decay data were collected over a 200 ns window and were each fit with biexponential functions. Notably, the samples with S- and Se-rich interfaces showed a decreased lifetime in the faster component when compared to control InP/ZnSe QDs. The As-rich interface sample exhibited very similar decay dynamics to the control InP/ZnSe QDs, while the P-rich interface sample showed a relatively larger magnitude of the slower time component, increasing the weighted lifetime. The decreased lifetime of the faster component observed for the chalcogenide-rich interfaces may suggest the emergence of new processes such as trapping at chalcogen-derived defect states. Lower PL QYs for samples with modified interfaces support the creation of new pathways that facilitate non-radiative recombination. While steady-state and time-resolved PL offer insight that a shifted atomic composition at the core/shell interface, even with submonolayer coverage, can alter the optical and photophysical properties in the ns timescale, the differences in the weighted lifetimes are small overall and show no change in the longer timescale. PL quenching evident in the overall low QY of the samples suggests behavior of the charge carriers not reflected in the observed lifetime and leads us to speculate that the ensembles contain populations of QDs that are non-luminescent. The creation of a permanently dark fraction upon shifting the stoichiometry at the core/shell interface is considered, given that such a shift could give rise to negatively charged QDs upon interstitial defect incorporation into the nanocrystal lattice. In doped QDs, the PL has been shown to be quenched by nonradiative Auger processes that are a few orders of magnitude faster than radiative recombination.[44,45] Given that the overall ensemble quantum yield is determined more dominantly by the dark fraction, this could also explain
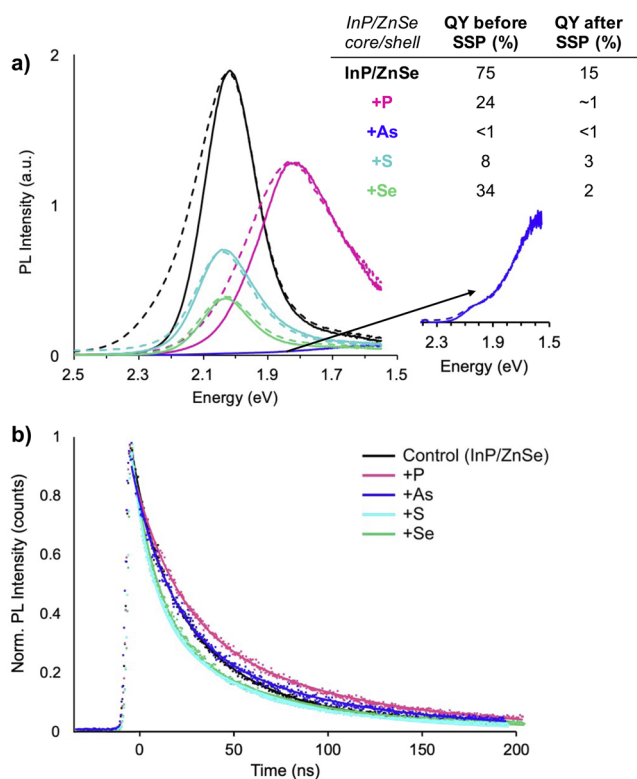

FIG. 2. (a) PL spectra of InP/ZnSe QDs with the anion-rich interface before size-selective precipitation (SSP) (dotted, normalized to solid trace) and after (solid) size-selective precipitation. Quantum yields before and after size-selective precipitation are noted in the legend. The InP + P/ZnSe sample quickly oxidized upon exposure to air precluding accurate measurement. (b) Excitonic PL decay dynamics of InP/ZnSe QDs with modulated interfaces measured at room temperature. Transient PL spectra were obtained by integrating streak camera data over 200 ns between 2.14 and 1.97 eV (black, navy, teal, and green traces) or 1.91 and 1.77 eV (pink trace).
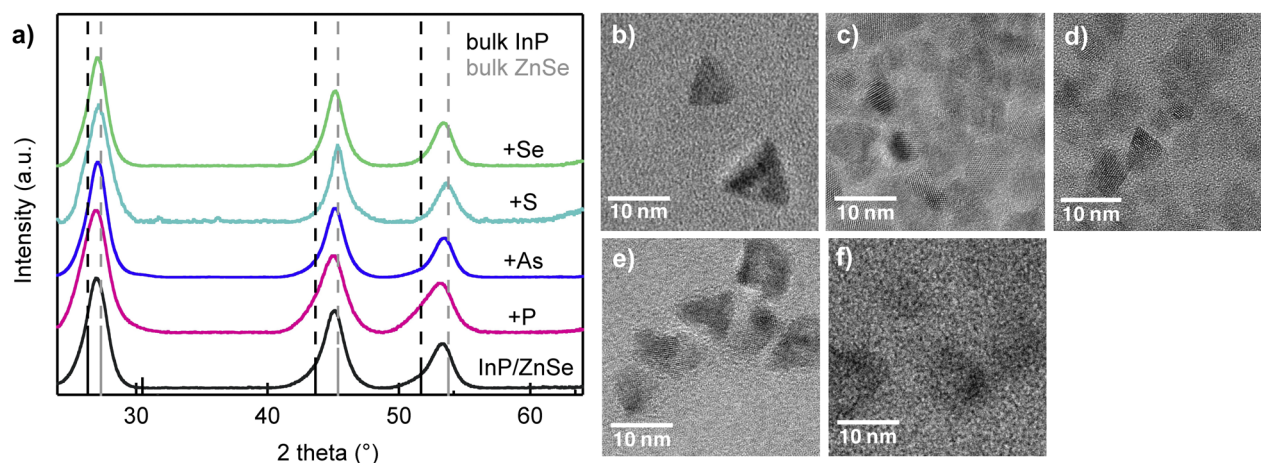
FIG. 3. (a) Powder XRD patterns of InP/ZnSe QDs with the anion-rich interface compared with traditional InP/ZnSe QDs exhibiting a shift from InP (PDF #01-070-2513) toward ZnSe (PDF #04-001-6858) and (b)–(f) TEM images of InP/ZnSe control, P, As, S, and Se-interface core/shell QDs.

the low QY of the anion-treated samples.[46] In light of recent NMR studies of Cd-treated InP QDs,[47] where the presence of a mixture of surface species including surface phosphates was confirmed, it seems that this approach to surface modification on an already defective core further reinforces the defect-ridden interface, resulting in poor optical properties. The removal of oxidized surface defects with HF and subsequent addition of anions was attempted and resulted in similar final PL QYs (Fig. S4), necessitating further exploration of the surface chemistry needed to form an ideal interface.

To better understand the nature of the trap states and the charge carrier dynamics, we measured the PL spectra at low temperature (77 K) to compare to room temperature PL (Fig. S5). Generally, it is evident that when the temperature is decreased, the excitonic PL blueshifts as expected from the Varshni relation.[48] For the samples with modulated interface compositions, the overall PL intensities tend to increase. Qualitatively, the relative increase in trap PL is higher than that of excitonic PL. This suggests a thermally mediated de-trapping mechanism at room temperature, which has been previously reported with InP cores with implication for defects from dangling bonds either from In or P surface atoms.[14] The anion-derived trap PL we observed in the surface modified InP cores is suppressed at room temperature upon shelling, but these electronic defects are evident in the low temperature spectra.

Tuning surface anion composition of optically bright, Zn-rich InP cores

We extended the sample set to include Zn-rich InP cores exhibiting 20% PL QY as the starting material for interface tuning and shelling. Zn-rich InP cores are best described as stoichiometric InP cores with Zn carboxylates as surface ligands. In this set of experiments, TMS phosphine and selenide were specifically chosen to modulate the interfacial stoichiometry. Additionally, as an analog to $Se(SiMe_3)_2$, TOP-Se was used for comparison. Upon introduction of the anion precursor, the absorption peak was redshifted across all samples accompanied by an increase in the PL intensity. With each subsequent addition of the shelling precursors, the absorption and PL maxima continued to redshift. The final absorption and PL wavelengths for these interface modified InP/ZnSe QDs were strikingly similar between In-rich and Zn-rich InP cores [Fig. S6(a)]. P-treated InP–Zn core QDs displayed the largest redshift overall, while surface treatment with $Se(SiMe_3)_2$ or TOP-Se resulted in PL maxima similar to what is observed for InP/ZnSe without surface anion treatment, with the overall PL profiles nearly overlapping. Starting with bright core QDs achieved with Zn treatment led to higher PL QYs in the final core/shell QDs overall and less loss of PL QY upon size-selective precipitation, suggesting that the emissive quality of the starting core material is critical to the final optical properties and photostability.

Elemental analysis by ICP-OES demonstrates that both P and Se introduced by the reactive silyl precursors were successfully incorporated into the final core/shell QDs (Table S1). In both cases, an overall anion-rich stoichiometry was obtained. Interestingly, there was a difference in the atomic ratios between the $Se(SiMe_3)_2$ and TOP-Se treated samples resulting in a reversed cation to anion ratio. This indicates that the reactive silyl precursor that targets direct reaction with surface carboxylates renders a different surface chemistry and atomic composition that persists after the shell growth. The expected zinc blende structure of the final core/shell QDs and the size and morphology of the particles were corroborated by the powder XRD patterns and TEM.

TABLE III. Parameters fit to the biexponential function for excitonic PL decay dynamics measured at room temperature.

Sample	A_1	τ_1 (ns)	A_2	τ_2 (ns)	$\tau_{weighted}$ (ns)
InP/ZnSe	0.61	19	0.35	67	37
InP + P/ZnSe	0.48	20	0.44	78	48
InP + As/ZnSe	0.55	19	0.36	76	38
InP + S/ZnSe	0.56	10	0.41	55	28
InP + Se/ZnSe	0.63	13	0.33	68	32

The excitonic PL decay dynamics of the InP/ZnSe QDs made from Zn-treated InP cores were investigated [Fig. S6(b) and Table S2]. Compared to the control InP/ZnSe sample, P-rich interface core/shell QDs showed a reduction in the amplitude of the short time component and a relative increase in the slower time component with an extended lifetime, similar to the decay dynamics when the In-rich InP core was shelled. The samples modified with Se precursors, however, exhibited very similar excitonic PL dynamics where the decay curve overlaps with that of the control InP/ZnSe sample. Here, the shift in stoichiometry of the cation to anion ratio induced by the different Se precursors evident in ICP-OES results does not have any observable changes in this timescale, suggesting that the loss in PL QY can again be attributed to hole-associated trapping on a faster timescale and the creation of non-radiative decay pathways and/or dark fractions. This also suggests that the immediate interface formed with the InP core (i.e., with Zn carboxylate) is more influential to the photophysics of heterostructure QDs. The dynamics in all of these systems remain remarkably similar. The low temperature PL of these samples (Fig. S5) shows a notably different trend from the samples made from In-rich InP cores. At lower temperature, the excitonic PL intensity decreased while the trap PL intensity increased. This is consistent with the observation of the InP/ZnSe control sample, supporting the importance of the immediate interfacial structure (surface anion vs cation) at the core/shell interface. Interestingly, the InP–Zn + P/ZnSe sample showed a redshift upon lowering the temperature, which to our knowledge has not previously been observed in shelled InP literature and is a surprising result, given the Varshni relation. While less common, an increase in bandgap with increasing temperature has been previously observed for Pb chalcogenide QDs and has been attributed to an unconventional trapped exciton state[49] or exciton dark-bright state splitting.[50]

Cluster-models of core and core/shell InP QDs

In order to gain further insight into the electronic structure of the surface modified core and core/shell QDs, we turned to density functional theory. Calculations were conducted using the Gaussian software package (G16.B01)[51] using the Perdew, Burke, and Ernzerhof hybrid functional (PBE0).[52–54] A quasi-spherical InP QD, $In_{77}P_{77}$ (diameter ~2 nm), was constructed using the bulk zinc blende crystal structure. The pure InP structure conformed to a C_{3v}
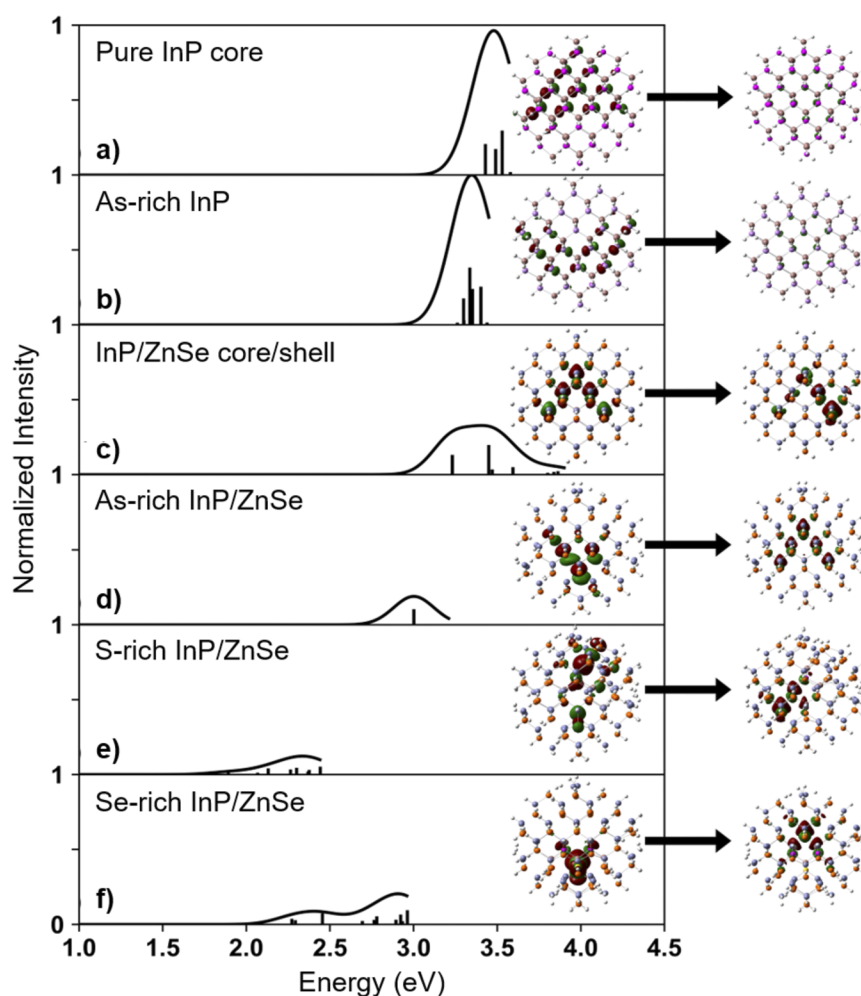

FIG. 4. The TD-DFT absorption spectra for (a) the stoichiometric $In_{77}P_{77}$ QD, (b) the As-rich $In_{77}P_{23}As_{54}$ QD, (c) the $In_{10}P_{10}/Zn_{67}Se_{67}$ core/shell QD, (d) the As-rich $In_{10}P_3As_7/Zn_{67}Se_{67}$ QD, (e) the S-rich $In_{10}P_4S_6/Zn_{67}Se_{67}$ QD, and (f) the Se-rich $In_{10}P_4Se_6/Zn_{67}Se_{67}$ QD. A smoothing function has been applied to the TD-DFT roots (shown as black vertical bars) of 0.12 eV and the resulting spectrum shown as the black line. Atoms are represented as balls with the In atoms in brown, the P atoms in pink, the S atoms in yellow, the Se atoms in orange, the As atoms in purple, the Zn atoms in gray, and the pseudo H as white. The leaving and arriving orbitals for the first bright transition (f > 0.01) for each system are plotted with an isovalue of 0.02 inset into the spectra. The energetic values for this transition are included in Table S3.

symmetry before optimization. Core/shell structures were built from the InP core by exchanging surface In with Zn and P with Se to form $In_{x-y}P_{x-y}/Zn_ySe_y$ (d ~ 2 nm for $In_{10}P_{10}/Zn_{67}Se_{67}$). In order to generate the anion-rich models ($In_{10}P_{10-y}E_y/Zn_{67}Se_{67}$, E = As, S, and Se), the previously optimized $In_{10}P_{10}/Zn_{67}Se_{67}$ core/shell model had the interfacial P atoms replaced. Surface dangling bonds were terminated using a pseudo-hydrogen capping scheme to compensate surface ions ($\pm 1/3$ for the non-shelled InP systems) resulting in the $(InP)_{77}H_{108}$ structure for the non-shelled system. The calculated bandgaps of the $(InP)_{77}H_{108}$ and the $(InP)_{10}/(ZnSe)_{67}H_{108}$ structures were 3.89 and 3.77 eV, respectively.

Surface modified core structures were constructed by replacing surface P atoms with As atoms resulting in an $In_{77}P_{23}As_{54}$ structure. The addition of the surface As atoms resulted in a decrease in the

bandgap (by 0.16 eV) in comparison to the $In_{77}P_{77}$ structure (Fig. 4 and Table S3). This resulted in a redshift in the time-dependent density functional theory (TD-DFT) absorption spectrum (by 0.13 eV), which is consistent with the experimental data. It is important to note that the models investigated are generally blueshifted in relation to the experimental systems as they are more quantum confined. Looking at the molecular orbitals (MOs) responsible for the transition for the As-rich system (Fig. 4 and Fig. S7), it is worth noting that there is little density at the surface where the replaced anions are located for either the HOMO or the LUMO, which is a possible explanation for why the observed redshift is minimal. In order to examine if additional localization can be achieved by the interfacial anion layer at the core/shell interface, the anion-modified models were shelled with ZnSe.
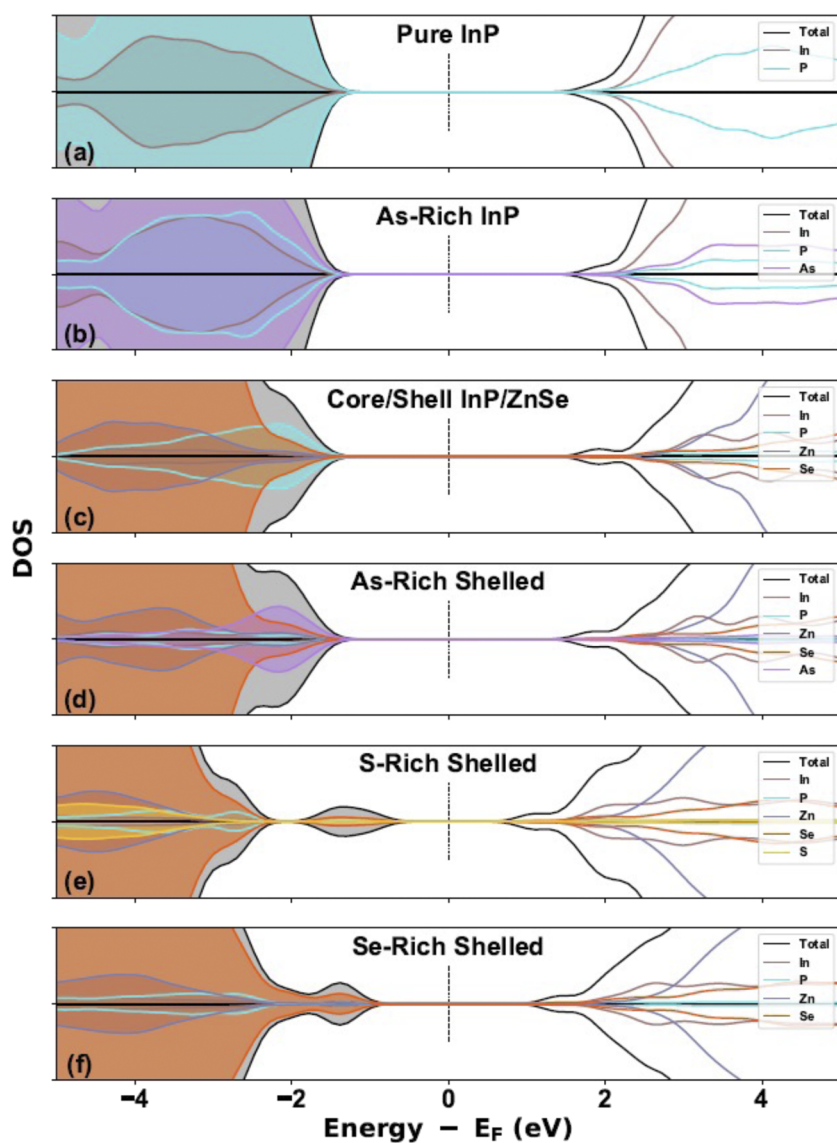

FIG. 5. The density of states plots for (a) the stoichiometric $In_{77}P_{77}$ QD, (b) the As-rich $In_{77}P_{23}As_{54}$ QD, (c) the $In_{10}P_{10}/Zn_{67}Se_{67}$ core/shell QD, (d) the As-rich $In_{10}P_3As_7/Zn_{67}Se_{67}$ QD, (e) the S-rich $In_{10}P_4S_6/Zn_{67}Se_{67}$ QD, and (f) the Se-rich $In_{10}P_4Se_6/Zn_{67}Se_{67}$ QD. The atomic P-orbital contributions by each atomic species are noted in color as contributing to the total density of states (in black). The DOS plots have had a gaussian smoothing of 0.2 eV applied. Positive and negative values correspond to spin up and down, respectively.

Upon the addition of the ZnSe shell to the InP system (going from $In_{77}P_{77}$ to $In_{10}P_{10}/Zn_{67}Se_{67}$), the bandgap for the system decreases (by 0.12 eV), as anticipated due to the ability for the wavefunction to diffuse into the shell. The addition of the anions to the core/shell structure results in an observable redshift of the TD-DFT absorption spectrum (Fig. 4). This corresponds to a reduction in the bandgaps due to the presence of the additional anions observed in all shelled structures (Fig. 5 and Table S3). Examination of the density of states (DOS) plot for the $In_{10}P_{10}/Zn_{67}Se_{67}$ structure (Fig. 5) shows that the states around the bandgap are comprised predominantly of P in the valence band and In in the conduction bands as expected for InP systems. However, due to the presence of the ZnSe shell, there are significant contributions by Se in the valence band and Zn in the conduction band, showing that the wavefunction is able to diffuse into the shell. The addition of As to the core/shell interface gives rise to As contributions in the valence band. These contributions work to reduce the bandgap (by 0.22 eV) from the $In_{10}P_{10}/Zn_{67}Se_{67}$ structure. This reduction in the bandgap is apparent in the computed TD-DFT absorption spectrum as a redshift (by 0.23 eV) similar to the process noted experimentally.

The addition of Se into the interface between the core and shell reduces the bandgap even further (by 1.02 eV) from the $In_{10}P_{10}/Zn_{67}Se_{67}$ structure. As shown in Fig. 5, Se contributes to states that begin to separate from the edge of the valence band and begin to form shallow hole-trap states resulting in the TD-DFT absorption spectrum being significantly redshifted (by 0.96 eV) from the $In_{10}P_{10}/Zn_{67}Se_{67}$ structure. The addition of S in the core/shell interface leads to a similar result, although the shifts are more pronounced (bandgap is redshifted by 1.62 eV and absorption is redshifted by 1.34 eV) as the states introduced to the band edge are further separated from the conduction band. It is important to note that similar band-edge states have been noted to form in computational InP cluster models before.[55] In this case, however, these states arose due to the surfaces of the InP models giving rise to spin densities localized to surface metal centers leading to high-spin ground states. To ensure this was not occurring, the energies of several (singlet, S = 0, through nonet, S = 8/2) were computed (Fig. S8), and it was found that the singlet configuration is the most stable. This is expected for these systems and indicates that there is a different mechanism for the appearance of these states.

Localization of the band-edge MOs to the anions was observed in the core/shell structures (Fig. S7). This localization introduces unique states in the doped systems that are dependent on the atomic composition of the core/shell interface. In the case of the As-rich system, these states are still within the conduction band; however, for the Se- and S-rich systems, these introduced states are above the conduction band, resulting in a significant redshift of the absorption spectrum and thus the appearance of hole-trap states that have been experimentally noted.

CONCLUSION AND FUTURE WORK

To summarize, we have synthesized a series of InP and InP/ZnSe QDs with anion-rich interfaces using reactive trimethylsilyl reagents and confirmed successful modification using NMR spectroscopy and elemental analysis. We have correlated these surface chemistry modifications with the resulting steady state and time-resolved PL properties of the QDs. UV–Vis and steady-state PL indicate that anion treatment of the InP cores induces delocalization of the exciton wavefunction and relaxation of core confinement. InP/ZnSe QDs prepared with modulated interfaces result in similar PL decay dynamics on the ns timescale, while the relatively low in PL QYs suggest the creation of new hole traps or non-radiative recombination channels, likely resulting in a permanently dark fraction. Although the standardized ZnSe shelling procedure did not result in improved PL properties for anion-doped InP QDs, we have successfully demonstrated surface-limited reaction chemistry with trimethylsilyl anion reagents as a method to deposit submonolayer inorganic shells and obtain a degree of control over shell growth and final absorption and PL profiles. These results introduce a useful method for interfacial control and show that the dynamics are not dramatically impacted at the ns timescale; however, PL QYs are still highly sensitive to interfacial composition. DFT calculations show that shallow hole traps are introduced that depend on the atomic composition of the core/shell interface. With increasing complexity and high applicability of QD materials, this work opens doors to atomistic control of the surface and interfaces of nanoscale materials.

SUPPLEMENTARY MATERIAL

Additional data, Figs. S1–S8, and computational details are available as the supplementary material.

ACKNOWLEDGMENTS

DATA AVAILABILITY

The data that support the findings of this study are available within the article and its supplementary material.

REFERENCES

[1] C. Ippen, W. Guo, D. Zehnder, D. Kim, J. Manders, D. Barrera, B. Newmeyer, D. Hamilton, C. Wang, C. Hotz, R. Ma, J. K. Bin, B. Kim, K. Kim, K. Jang, J. Park, T. Lee, W. Y. Kim, and J. Lee, J. Soc. Inf. Disp. **27**, 338 (2019).

[2] J.-H. Jo, J.-H. Kim, K.-H. Lee, C.-Y. Han, E.-P. Jang, Y. R. Do, and H. Yang, Opt. Lett. **41**, 3984 (2016).

[3] J. Lim, M. Park, W. K. Bae, D. Lee, S. Lee, C. Lee, and K. Char, ACS Nano **7**, 9019 (2013).

[4] Y. Kim, S. Ham, H. Jang, J. H. Min, H. Chung, J. Lee, D. Kim, and E. Jang, ACS Appl. Nano Mater. **2**, 1496 (2019).

[5] H. Zhang, X. Ma, Q. Lin, Z. Zeng, H. Wang, L. S. Li, H. Shen, Y. Jia, and Z. Du, J. Phys. Chem. Lett. **11**, 960 (2020).

[6] T. Lee, D. Hahm, K. Kim, W. K. Bae, C. Lee, and J. Kwak, Small **15**, 1905162 (2019).

[7] Y.-H. Won, O. Cho, T. Kim, D.-Y. Chung, T. Kim, H. Chung, H. Jang, J. Lee, D. Kim, and E. Jang, Nature **575**, 634 (2019).

[8] Y. Li, X. Hou, X. Dai, Z. Yao, L. Lv, Y. Jin, and X. Peng, J. Am. Chem. Soc. **141**, 6448 (2019).

[9] H. Fu and A. Zunger, Phys. Rev. B **56**, 1496 (1997).

[10] S. Adam, D. V. Talapin, H. Borchert, A. Lobo, C. McGinley, A. R. B. de Castro, M. Haase, H. Weller, and T. Möller, J. Chem. Phys. **123**, 084706 (2005).

[11] S. V. Kilina, P. K. Tamukong, and D. S. Kilin, Acc. Chem. Res. **49**, 2127 (2016).

[12] C. Giansante and I. Infante, J. Phys. Chem. Lett. **8**, 5209 (2017).

[13] A. J. Houtepen, Z. Hens, J. S. Owen, and I. Infante, Chem. Mater. **29**, 752 (2017).

[14] E. Cho, T. Kim, S.-m. Choi, H. Jang, K. Min, and E. Jang, ACS Appl. Nano Mater. **1**, 7106 (2018).

[15] M. V. Kovalenko, M. Scheele, and D. V. Talapin, Science **324**, 1417 (2009).

[16] M. T. Frederick and E. A. Weiss, ACS Nano **4**, 3195 (2010).

[17] B. M. Cossairt, P. Juhas, S. J. L. Billinge, and J. S. Owen, J. Phys. Chem. Lett. **2**, 3075 (2011).

[18] S. Jin, R. D. Harris, B. Lau, K. O. Aruda, V. A. Amin, and E. A. Weiss, Nano Lett. **14**, 5323 (2014).

[19] J.-Y. Kim and N. A. Kotov, Chem. Mater. **26**, 134 (2014).

[20] M. A. Boles, D. Ling, T. Hyeon, and D. V. Talapin, Nat. Mater. **15**, 141 (2016).

[21] J. L. Stein, E. A. Mader, and B. M. Cossairt, J. Phys. Chem. Lett. **7**, 1315 (2016).

[22] T.-G. Kim, D. Zherebetskyy, Y. Bekenstein, M. H. Oh, L.-W. Wang, E. Jang, and A. P. Alivisatos, ACS Nano **12**, 11529 (2018).

[23] K. E. Hughes, J. L. Stein, M. R. Friedfeld, B. M. Cossairt, and D. R. Gamelin, ACS Nano **13**, 14198 (2019).

[24] R. Toufanian, A. Piryatinski, A. H. Mahler, R. Iyer, J. A. Hollingsworth, and A. M. Dennis, Front. Chem. **6**, 567 (2018).

[25] E. Jang, Y. Kim, Y.-H. Won, H. Jang, and S.-M. Choi, ACS Energy Lett. **5**, 1316 (2020).

[26] F. Cao, S. Wang, F. Wang, Q. Wu, D. Zhao, and X. Yang, Chem. Mater. **30**, 8002 (2018).

[27] F. Pietra, L. De Trizio, A. W. Hoekstra, N. Renaud, M. Prato, F. C. Grozema, P. J. Baesjou, R. Koole, L. Manna, and A. J. Houtepen, ACS Nano **10**, 4754 (2016).

[28] J. T. Mulder, N. Kirkwood, L. De Trizio, C. Li, S. Bals, L. Manna, and A. J. Houtepen, ACS Appl. Nano Mater. **3**, 3859 (2020).

[29] Y.-S. Park, W. K. Bae, L. A. Padilha, J. M. Pietryga, and V. I. Klimov, Nano Lett. **14**, 396 (2014).

[30] N. J. Freymeyer, S. M. Click, K. R. Reid, M. F. Chisholm, C. E. Bradsher, J. R. McBride, and S. J. Rosenthal, J. Chem. Phys. **152**, 161104 (2020).

[31] P. Rodosthenous, F. M. Gómez-Campos, and M. Califano, J. Phys. Chem. Lett. **11**, 10124 (2020).

[32] M. Rusishvili, S. Wippermann, D. V. Talapin, and G. Galli, Chem. Mater. **32**, 9798 (2020).

[33] Q. Zhao and H. J. Kulik, Chem. Mater. **30**, 7154 (2018).

[34] D. C. Gary and B. M. Cossairt, Chem. Mater. **25**, 2463 (2013).

[35] P. E. Chen, N. C. Anderson, Z. M. Norman, and J. S. Owen, J. Am. Chem. Soc. **139**, 3227 (2017).

[36] A. Ritchhart and B. M. Cossairt, Inorg. Chem. **58**, 2840 (2019).

[37] S.-W. Kim, J. P. Zimmer, S. Ohnishi, J. B. Tracy, J. V. Frangioni, and M. G. Bawendi, J. Am. Chem. Soc. **127**, 10526 (2005).

[38] J. J. Buckley, E. Couderc, M. J. Greaney, J. Munteanu, C. T. Riche, S. E. Bradforth, and R. L. Brutchey, ACS Nano **8**, 2512 (2014).

[39] C. M. Gentle, Y. Wang, T. N. Haddock, C. P. Dykstra, and R. M. van der Veen, J. Phys. Chem. C **124**, 3895 (2020).

[40] P. Ramvall, S. Tanaka, S. Nomura, P. Riblet, and Y. Aoyagi, Appl. Phys. Lett. **73**, 1104 (1998).

[41] J. O. V. Monchen, R. W. Crisp, G. Grimaldi, H. A. C. Bergstein, I. du Fossé, W. van der Stam, I. Infante, and A. J. Houtepen, J. Am. Chem. Soc. **140**, 15712 (2018).

[42] C. F. Holder and R. E. Schaak, ACS Nano **13**, 7359 (2019).

[43] A. Sarkar, P. Mukherjee, and P. Barat, Mater. Sci. Eng., A **485**, 176 (2008).

[44] Al. L. Efros and M. Rosen, Phys. Rev. Lett. **78**, 1110 (1997).

[45] P. A. Frantsuzov and R. A. Marcus, Phys. Rev. B **72**, 155321 (2005).

[46] C. D. Heyes, A. Yu. Kobitski, V. V. Breus, and G. U. Nienhaus, Phys. Rev. B **75**, 125431 (2007).

[47] M. P. Hanrahan, J. L. Stein, N. Park, B. M. Cossairt, and A. J. Rossini, J. Phys. Chem. C **125**, 2956 (2021).

[48] I. A. Vainshtein, A. F. Zatsepin, and V. S. Kortov, Phys. Solid State **41**, 905 (1999).

[49] J. E. Lewis, S. Wu, and X. J. Jiang, Nanotechnology **21**, 455402 (2010).

[50] M. S. Gaponenko, N. A. Tolstik, A. A. Lutich, A. A. Onushchenko, and K. V. Yumashev, Physica E **53**, 63 (2013).

[51] M. J. Frisch, G. W. Trucks, H. B. Schlegel, G. E. Scuseria, M. A. Robb, J. R. Cheeseman, G. Scalmani, V. Barone, G. A. Petersson, H. Nakatsuji, X. Li, M. Caricato, A. V. Marenich, J. Bloino, B. G. Janesko, R. Gomperts, B. Mennucci, H. P. Hratchian, J. V. Ortiz, A. F. Izmaylov, J. L. Sonnenberg, D. Williams-Young, F. Ding, F. Lipparini, F. Egidi, J. Goings, B. Peng, A. Petrone, T. Henderson, D. Ranasinghe, V. G. Zakrzewski, J. Gao, N. Rega, G. Zheng, W. Liang, M. Hada, M. Ehara, K. Toyota, R. Fukuda, J. Hasegawa, M. Ishida, T. Nakajima, Y. Honda, O. Kitao, H. Nakai, T. Vreven, K. Throssell, J. A. Montgomery, Jr., J. E. Peralta, F. Ogliaro, M. J. Bearpark, J. J. Heyd, E. N. Brothers, K. N. Kudin, V. N. Staroverov, T. A. Keith, R. Kobayashi, J. Normand, K. Raghavachari, A. P. Rendell, J. C. Burant, S. S. Iyengar, J. Tomasi, M. Cossi, J. M. Millam, M. Klene, C. Adamo, R. Cammi, J. W. Ochterski, R. L. Martin, K. Morokuma, O. Farkas, and J. B. Foresman, and D. J. Fox, Gaussian 16, Revision B.01, 2016.

[52] J. P. Perdew, K. Burke, and M. Ernzerhof, Phys. Rev. Lett. **78**, 1396 (1997).

[53] M. Ernzerhof and G. E. Scuseria, J. Chem. Phys. **110**, 5029 (1999).

[54] C. Adamo and V. Barone, J. Chem. Phys. **110**, 6158 (1999).

[55] P. T. Snee, J. Phys. Chem. C **125**, 11765 (2021).